ELSEVIER

Microporous and Mesoporous Materials 33 (1999) 61–75

MICROPOROUS AND MESOPOROUS MATERIALS

www.elsevier.nl/locate/micmat

# Effect of manganese substitution on the physicochemical properties and catalytic toluene oxidation activities of Mg–Al layered double hydroxides

S. Velu *, N. Shah [1], T.M. Jyothi, S. Sivasanker

*Catalysis Division, National Chemical Laboratory, Pune 411 008, India*

Received 3 December 1998; received in revised form 8 April 1999; accepted for publication 4 June 1999

**Abstract**

A series of Mg–Mn–Al ternary hydrotalcite-like layered double hydroxides (LDHs) with (Mg + Mn)/Al atomic ratios of ~3 and Mg:Mn atomic ratios ranging from 3:0 to 0:3 were synthesized by a co-precipitation method. The incorporation of Mn in the MgAl-LDH was investigated by employing various techniques, such as powder X-ray diffraction, Fourier transform infrared spectroscopy, electron paramagnetic resonance (EPR) spectroscopy, UV–visible diffuse-reflectance spectroscopy (UV–Vis DRS) and thermogravimetry. A single phase corresponding to LDH was obtained up to the composition Mg:Mn:Al = 2.2:0.8:1. A further increase in the Mn content resulted in the formation of a mixture of LDH, $Mn(OH)_2$ and $MnCO_3$ phases. Partial oxidation of $Mn^{2+}$ to $Mn^{3+}$ took place during synthesis, as evidenced by UV–Vis DRS. According to the EPR and UV–Vis DRS results, the $Mn^{2+}/Mn^{3+}$ ions were present in a (distorted) octahedral environment. Calcination at 723 K resulted in the formation of a poorly crystalline MgO-like solid solution. Mn retained its +2 oxidation state (EPR active) even upon calcination at very high temperature (1473 K) in air. At a higher Mn content, in addition to the MgO-like phase, spinel phases such as $Mn_3O_4$ and $MnAl_2O_4$ were also obtained at 723 K. The catalytic activity of the as-synthesized samples was tested in the liquid-phase oxidation of toluene using *tert*-butyl hydroperoxide as the oxidant. Benzaldehyde and benzoic acid were the major products with minor amounts of benzyl alcohol. The compound without an LDH phase was found to be less active for the oxidation of toluene under similar reaction conditions. Solvents were found to have a profound influence on the catalytic activity and the product selectivity. 

*Keywords:* Anionic clays; Hydrotalcites; Layered double hydroxides; Manganese oxide; Mesoporous materials; Mn incorporation; Toluene oxidation

* Corresponding author. Present address: Ceramics Technology Department, National Industrial Research Institute of Nagoya, Nagoya-462, Japan. Fax: +81-52-911-2111.

*E-mail address:* subrama@nirin.go.jp (S. Velu)

[1] Present address: Institut für Anorganische Chemie, RWTH-Aachen, Germany.

1387-1811/99/$ - see front matter 
PII: S1387-1811(99)00123-7

## 1. Introduction

Manganese is an essential component in photosynthetic systems [1]. It is also known to be a necessary element in various biological systems, and its redox chemistry is especially important in electron transfer reactions [2]. Owing to its ability to display variable oxidation states (+2, +3, +4 and +7) the manganese-based mixed oxide systems serve as efficient catalysts in many industrially important oxidation processes, such as the oxidation of CO, methanol, ethylene, ammonia, nitric oxide and combustion reactions [3–5].

On the other hand, layered double hydroxides (LDHs) or synthetic anionic clays having a hydrotalcite (HT)-like structure have attracted increasing attention in recent years owing to their potential industrial applications as ion exchangers, adsorbents, ionic conductors, catalysts and catalyst supports [6]. The crystal structure of LDHs consists of positively charged brucite [$Mg(OH)_2$]-like octahedral layers, in which a part of the M(II) cations are isomorphously substituted by an M(III) cation. Interstitial layers built of $CO_3^{2-}$ anions and crystal water compensate the excess positive charge of the octahedral layers resulting from this substitution. The naturally occurring anionic clay has the formula $Mg_6Al_2(OH)_{16}CO_3 \cdot 4H_2O$ [6]. Both Mg and Al can be isomorphously substituted by divalent cations like Cu, Ni, Co, Zn, or trivalent cations such as Fe, Cr, Ga, Rh [7–9], or even tetravalent cations, for example Zr [10] and Sn [11], in order to expand the potential utility of these materials. Hence, a large number of LDHs with a wide variety of M(II)–M(III) cation pairs, as well as an M(I)–M(III) cation pair (e.g. Li–Al), with different anions in the interlayer has been reported in the scientific literature. However, LDHs containing $Mn^{2+}/Mn^{3+}$ in the brucite-like layer are scarce. The existence of 'desautelsite', a naturally occurring MgMn-LDH, was described by Dunn et al. [12]. Hansen and Taylor [13] synthesized a binary MgMn-LDH by air oxidation of $MnCO_3$ in $Mg(NO_3)_2$ at a constant pH ~ 9 (induced hydrolysis method). Later, Fernandez et al. [14] synthesized the same compound by a co-precipitation method using a mixture of $Mg(NO_3)_2$ and $MnCl_2$. From temperature-programmed reduction studies they estimated that 84% of the $Mn^{2+}$ had oxidized to $Mn^{3+}$ during the synthesis process. However, until now, no report is available on the synthesis, physicochemical and catalytic properties of a ternary LDH containing manganese in the Mg–Al brucite-like layer [15].

In the present study we have synthesized a new series of Mg–Mn–Al ternary-LDHs by a simple co-precipitation method. The changes in the physicochemical properties and the nature of Mn species present in the MgAl-LDH were investigated employing various spectroscopic and analytical techniques. We also report here for the first time on the catalytic performance of these Mn-incorporated LDHs in the liquid-phase oxidation of toluene.

## 2. Experimental

### 2.1. Synthesis of Mn-substituted LDHs

A series of magnesium–manganese–aluminum LDHs with (Mg + Mn)/Al = 3 and different Mg:Mn atomic ratios (3:0 to 0:3) were synthesized by a co-precipitation method [10]. Two aqueous solutions, one containing a mixture of $Mg(NO_3)_2$, $Al(NO_3)_3$ and $MnCl_2$ and the other containing a mixture of $NaOH/Na_2CO_3$, were added dropwise at room temperature while the pH was maintained between 9 and 10. The resulting slurry was digested at 338 K for 30 min. The precipitate was washed with hot distilled water until the pH of the filtrate was around 7. The precipitate was then dried in an oven at 373 K for 8 h.

### 2.2. Techniques

Powder X-ray diffraction (XRD) patterns of the as-synthesized samples were obtained using a Philips Norelco (Model PW 1730) diffractometer, and a Rigaku (model D-MAX III VC) X-ray unit was employed for the calcined samples. For qualitative identification of the phases present, the patterns were taken at a scan speed of $2\theta = 2^\circ$/min, whereas a speed of $0.5^\circ$/min was used for the calculation of the lattice parameters. Elemental Si

was used as an internal standard to correct the observed $2\theta$ values. The IR spectra were recorded on a Nicolet 60-SXB Fourier transform IR (FT-IR) spectrometer in the region 4000–400 $cm^{-1}$ using KBr pellets. Measurements were made in the region 200–900 nm using diffuse-reflectance spectroscopy (DRS) of all the Mn-incorporated LDH samples using a Shimadzu UV–visible spectrophotometer (model 2101-PC). Pure magnesium–aluminum LDH with an atomic ratio of Mg/Al = 3 (Mn 0.0-LDH), which exhibited a very weak absorption around 200 nm, was used as a secondary reference to correct the background of the spectrum. Electron paramagnetic resonance (EPR) spectra were collected using an X-band ($v = 9.75$ GHz) EPR spectrometer (Bruker model ER 200D-SRC) at room temperature or at 77 K. The magnetic field was swept starting from 1000 G. Thermogravimetric measurements of these compounds were performed in a Seiko Instrument TG/DTA model 32, in the temperature range 323–1173 K at a heating rate of 10 K/min under an $N_2$ atmosphere. The surface areas of both uncalcined and calcined samples (723 K) were measured by the BET method using $N_2$ as an adsorbate at 77 K (Coulter 100 CX Omnisorb).

### 2.3. Catalytic studies

The liquid-phase oxidation of toluene was carried out in a two-necked round bottom flask equipped with a reflux condenser. Acetonitrile (solvent, 10 ml) and 500 mg of toluene (5.43 mmol) were magnetically stirred at 353 K. The catalyst (50 or 100 mg) was added to the flask, followed by dropwise addition of 2.8 g of *tert*-butyl hydroperoxide (TBHP, 70% aqueous solution, Aldrich; 21.71 mmol). After 5 h reaction time, the reaction products were analyzed by gas chromatography using an SE 30 capillary column and a flame ionization detector.

## 3. Results and discussion

### 3.1. Mn-incorporated LDHs

The XRD patterns of some of the manganese-substituted LDHs are presented in Fig. 1. A single

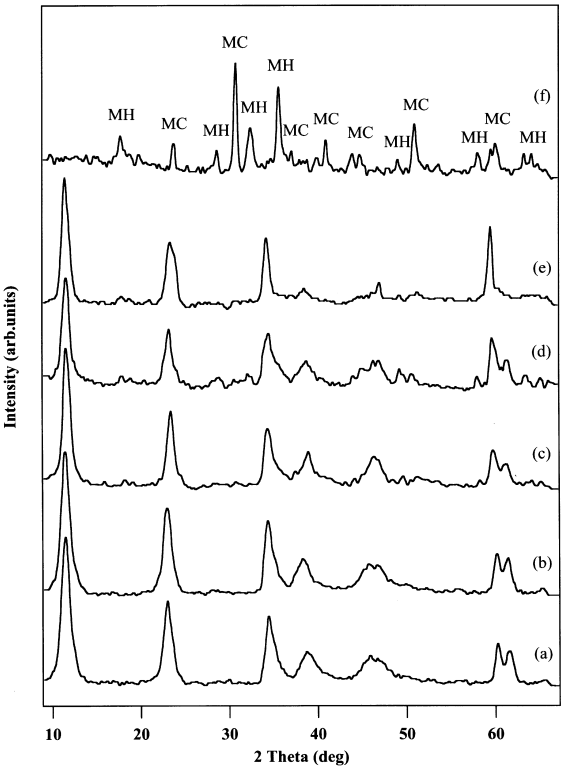


Fig. 1. XRD patterns of (a) Mn 0.0-LDH, (b) Mn 0.05-LDH, (c) Mn 0.8-LDH, (d) Mn 1.5-LDH, (e) Mn 2.0-LDH, (f) Mn 3.0-LDH; MC = $MnCO_3$; MH = $Mn(OH)_2$.

phase corresponding to HT-like LDH is obtained in the composition range Mg:Mn:Al = 3.0:0.0:1 to 2.2:0.8:1 (Mn 0.0-LDH to Mn 0.8-LDH; Table 1). A further increase in the Mn content results in the appearance of small impurity peaks corresponding to pyrochroite [$Mn(OH)_2$; JCPDS file no. 18-788a] and rhodochrosite [$MnCO_3$; JCPDS file no. 7-270) phases in addition to the LDH phase. The compound without Mg (Mn 3.0-LDH) shows only a mixture of $Mn(OH)_2$ and $MnCO_3$ phases. No LDH phase is detected under our experimental conditions, although the existence of a binary MnAl-LDH is known in the literature [16]. Hence, there should be a limitation on the amount of Mn incorporation in the MgAl-LDH framework. Our results (with Mn 0.8-LDH) reveal that about 20% of the metal ions ($Mg^{2+}/Al^{3+}$) can be isomorphously substituted by Mn in the Mg–Al brucite-like layer to obtain a single phase corresponding

Table 1
Chemical composition, lattice parameters and surface areas of MgMnAl-LDHs

| Compound | Mg:Mn:Al atomic ratio | Mg/Mn atomic ratio | XRD phase obtained[a] | FWHM of (003) peak ($2\theta$) | Lattice parameter[b] (Å) | | BET surface area[c] ($m^2\ g^{-1}$) |
|---|---|---|---|---|---|---|---|
| | | | | | *a* | *c* | |
| Mn 0.0-LDH | 3.0:0.0:1 | – | LDH | 0.620 | 3.041 | 22.956 | 40 |
| Mn 0.05-LDH | 2.95:0.05:1 | 59 | LDH | 0.649 | 3.041 | 22.956 | 53 |
| Mn 0.8-LDH | 2.2:0.8:1 | 2.75 | LDH | 0.738 | 3.049 | 22.893 | – |
| Mn 1.0-LDH | 2.0:1.0:1 | 2.0 | LDH + MH | – | 3.049 | 22.827 | 48 |
| Mn 1.5-LDH | 1.5:1.5:1 | 1.0 | LDH + MH + MC | 0.880 | 3.054 | 22.727 | 62 |
| Mn 2.0-LDH | 1.0:2.0:1 | 0.5 | LDH + MH + MC | 0.885 | 3.059 | 22.656 | 60 |
| Mn 3.0-LDH | 0.0:3.0:1 | – | MH + MC | – | – | – | – |

[a] LDH = layered double hydroxide; MH = $Mn(OH)_2$ (JCPDS file no. 18-788a); MC = $MnCO_3$ (JCPDS file no. 7-270).
[b] Lattice parameter of the LDH phase calculated by the least squares method.
[c] BET surface area of samples degassed at 373 K.

to the LDH [(Mg + Al)/Mn = 4; Mg/Mn = 2.75]. This composition is similar to the composition of the 'desautelsite' clay, without Al, [Mg(II)Mn-(III)-LDH; $Mg^{2+}/Mn^{3+} \approx 3$] synthesized by a similar co-precipitation method [14]. A further increase in the Mn content in our system results in the co-formation of $Mn(OH)_2/MnCO_3$ phases. It is also possible that a part of the $Mn^{2+}$ is oxidized to $Mn^{3+}$ or $Mn^{4+}$ under our experimental conditions, since, according to the redox potentials, the oxidation of $Mn^{2+}$ to $Mn^{3+}$ is highly favorable in a basic medium $\{E^0[Mn(OH)_3/Mn(OH)_2] = 0.1\ V\}$ [17]. However, the XRD of our samples did not show any phase corresponding to either $Mn^{3+}$- or $Mn^{4+}$-containing compounds. If they were formed they might be isomorphously present in the brucite-like layer, because of their favorable ionic radii (the ionic radii of $Mn^{3+}$ and $Mn^{4+}$ in a high spin environment are 0.65 Å and 0.54 Å, respectively, and those of $Mg^{2+}$ and $Al^{3+}$ are 0.72 Å and 0.53 Å, respectively) [18]. The crystallographic parameters *a* and *c* of the LDH phase were calculated using the least squares method assuming a hexagonal crystal system. The results are reported in Table 1. It can be seen that there is a small increase in the *a* value with increasing Mn content, suggesting that a part of the $Mg^{2+}$ is being isomorphously substituted by $Mn^{2+}$ in the LDH framework. In contrast, the parameter *c*, which depends upon several factors, such as the amount of interlayer water, crystallinity of the compound and the extent of interaction between the layer and the interlayer, seems to be decreasing with increasing Mn content. Since the synthetic parameters were kept constant for all the compounds, while varying only the composition of the metal ions, the decrease in the *c* parameter is probably due to an increase in the electrostatic attractive forces between the layer and the interlayer. This is possible if a metal in higher oxidation states ($M^{3+}$ or $M^{4+}$) is isomorphously present in the brucite-like layer. We observed similar results upon incorporation of $Sn^{4+}$ in the MgAl-LDH system [11]. Hence, we tentatively attribute the decrease in the *c* parameter to an isomorphous incorporation of $Mn^{3+}$ or $Mn^{4+}$ along with $Mn^{2+}$ in the brucite-like layer. However, the lattice parameters continue to change even beyond Mn 0.8-LDH, which may be due to the uncertainty in determining the peak positions because of the low crystallinity of the samples.

The full width at half maximum (FWHM) of the (003) plane ($2\theta \approx 12^\circ$) is also included in Table 1 as a measure of crystallinity of the LDH phase in the *c*-axis direction. It can be seen that the FWHM value increases with increasing Mn content, demonstrating that the crystallinity of the LDH phase decreases due to the distortion induced by the substitution of Mn in the MgAl-LDH framework.

The FT-IR spectra of MgAl-LDH (without Mn) showed [19] strong absorption bands in the

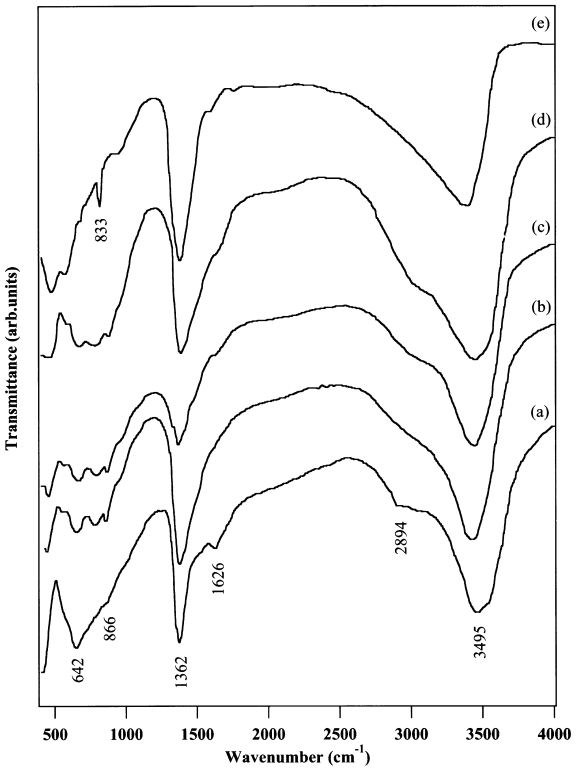


Fig. 2. FT-IR spectra of (a) Mn 0.05-LDH, (b) Mn 0.8-LDH, (c) Mn 1.5-LDH, (d) Mn 2.0-LDH, (e) Mn 3.0-LDH.

range 3440–3550 $cm^{-1}$ due to the hydroxyl (OH) stretching vibration, and the corresponding deformation mode appeared around 1600 $cm^{-1}$. IR absorptions due to the $v_2$, $v_3$ and $v_4$ stretching vibrations of interlayer $CO_3^{2-}$ ions were recorded around 870 $cm^{-1}$, 1360 $cm^{-1}$ and 640 $cm^{-1}$, respectively. The Mn-substituted LDHs show similar IR features (see Fig. 2). However, differences are noticed in the intensity and the sharpness of the bands upon manganese incorporation. For example, the sharpness of both $v_{OH}$ and $v_3$ of $CO_3^{2-}$ decreases (broadness of the band increases) with increasing Mn content. The intensity of a weak shoulder around 2900 $cm^{-1}$ due to water molecules hydrogen-bonded to interlayer $CO_3^{2-}$ ions decreases and the band shifts toward higher wavenumbers. These changes may be due to the co-formation of $Mn(OH)_2$ and $MnCO_3$ phases along with the LDH phase at higher Mn contents. The FT-IR spectra of Mn 3-LDH, the XRD of which showed only a mixture of $Mn(OH)_2$ and $MnCO_3$, exhibits a strong band around 830 $cm^{-1}$ for $v_3$ of $MnCO_3$ [13]. The $v_4$ band of interlayer $CO_3^{2-}$ that appears around 640 $cm^{-1}$ is absent in this sample, because of the absence of the LDH structure.

Table 2
Literature data on charge-transfer and d–d transfer transitions of some reference compounds

| Compound | $Mn^{n+}$ | $\lambda_{max}$ (nm) | Assignment | Reference |
|---|---|---|---|---|
| MnO | $Mn^{2+}$ | 420 | $^6A_{1g}\rightarrow{}^4A_{1g}$ | [20] |
| | | 500 | $^6A_{1g}\rightarrow{}^4T_{2g}$ | |
| | | 610 | $^6A_{1g}\rightarrow{}^4T_{2g}$ | |
| $Mn_3O_4$ | $Mn^{2+}$ | 255 | $O^{2-}\rightarrow Mn^{2+}$ | [21] |
| | $Mn^{3+}$ | 320 | $O^{2-}\rightarrow Mn^{3+}$ | |
| $Mn_2O_3$ | $Mn^{3+}$ | 370 | $^5B_{1g}\rightarrow{}^5B_{2g}$ | [21] |
| | | 485 | $^5B_{1g}\rightarrow{}^5E_g$ | |
| | | 755 | $^5B_{1g}\rightarrow{}^5A_{1g}$ | |
| Mn–$Al_2O_3$ | $Mn^{2+}$ | 422 | $^6A_{1g}\rightarrow{}^4A_{1g}$ | [22] |
| | $Mn^{3+}$ | 485 | $^5E_g\rightarrow{}^5T_{2g}$ | |
| | $Mn^{4+}$ | 470 | $^4A_{2g}\rightarrow{}^4T_{2g}$ | |

UV–Vis DRS can provide information regarding the oxidation state of manganese and its chemical environment. Table 2 gives some literature data on the absorption bands of d–d transitions of manganese in different chemical environments. The d–d transitions of $Mn^{3+}$ and $Mn^{4+}$ can be clearly identified in the UV–Vis region, whereas the transitions due to $Mn^{2+}$ ions are, in principle, both spin- and orbital-forbidden and, as a consequence, are weak.

The UV–Vis DRS results of some of the Mn-containing LDHs are shown in Fig. 3. The compound with the lowest Mn content (Mn 0.05-LDH) exhibits an intense band around 250 nm that can be assigned to the $O^{2-}\rightarrow Mn^{2+}$ charge transfer transition (see Table 2). Weak bands around 420 nm and 500 nm are also found, which are assigned to the $^6A_{1g}\rightarrow{}^4A_{1g}$ and $^6A_{1g}\rightarrow{}^4T_{2g}$ crystal field transitions, respectively. As the Mn content in the sample increases, the intensity of all these bands increases as well. An additional broad band in the region 320–380 nm is accompanied by weak shoulders around 480 and 800 nm. This band is in the same region as those reported for charge transfer and d–d transfer trans-

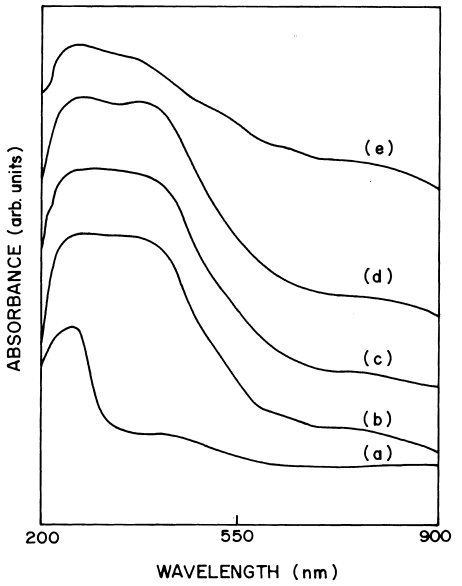


Fig. 3. UV–Vis DRS of (a) Mn 0.05-LDH, (b) Mn 1.0-LDH, (c) Mn 1.5-LDH, (d) Mn 2.0-LDH, (e) Mn 3.0-LDH.

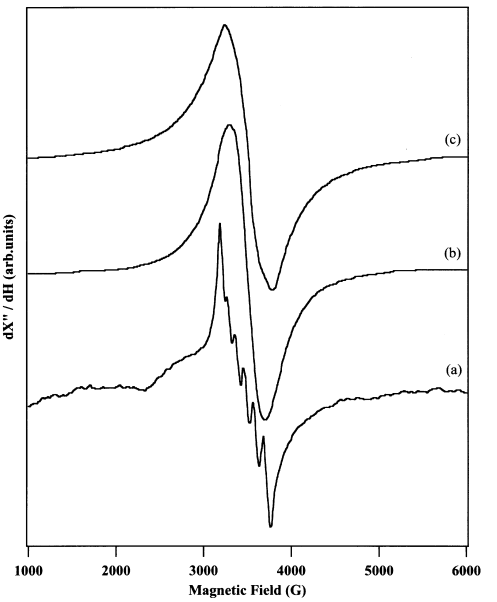


Fig. 4. EPR spectra of (a) Mn 0.05-LDH, (b) Mn 0.8-LDH, (c) Mn 1.5-LDH.

itions of $Mn_2O_3$ (see Table 2). Based on the literature data [21], the broad band in the range 320–380 nm and the weak shoulder around 480 nm are assigned to the $O^{2-} \rightarrow Mn^{3+}$ charge transfer transition superimposed on $^5B_{1g} \rightarrow {}^5B_{2g}$ and $^5B_{1g} \rightarrow {}^5E_g$ crystal field d–d transitions, respectively. The weak band around 800 nm is due to the $^5B_{1g} \rightarrow {}^5A_{1g}$ d–d transition in the $Mn^{3+}$ ion. Therefore, the UV–Vis DRS results suggest that Mn is present mostly as $Mn^{2+}$ in Mn 0.05-LDH, whereas partial oxidation to $Mn^{3+}$ and/or $Mn^{4+}$ is taking place upon increasing the Mn content in the sample.

EPR spectroscopy has been employed to corroborate further the UV–Vis DRS results on the oxidation states and the chemical environment of Mn species present in these samples. Usually, $Mn^{3+}$ is EPR silent owing to its large zero-field splitting [23,24]. Both $Mn^{2+}$ and $Mn^{4+}$ can give similar EPR spectra. The $Mn^{2+}$ in Mn–MCM-41 [23,24], as well as in Mn-containing aluminophosphates (MnAPOs) [25,26], showed six hyperfine lines with a $g$ value of around 2.0. The hyperfine coupling constant $A$ was in the range 80–100 G. On the other hand, $Mn^{4+}$ showed a $g$ value of less than 2 and an $A$ value of around 76 G. Hence, with the help of EPR it may be possible to identify the presence of $Mn^{2+}$ and/or $Mn^{4+}$ species in these compounds [22,27,28].

The X-band EPR spectra of various Mn-containing LDHs measured at room temperature are depicted in Fig. 4. For the sample with the lowest Mn content (Mn 0.05-LDH), the EPR spectrum shows six hyperfine lines centered around $g = 2.0147$ [Fig. 4(a)], indicating the existence of $Mn^{2+}$ ions. However, the sextet lines are not equally spaced; the spacing increases from 80 to 120 G with increasing magnetic field. In addition, the line height of the sextet varies considerably. A closer observation reveals some shoulders between the major hyperfine lines. These shoulders originate either from the presence of additional $Mn^{2+}$ species or from forbidden transitions [25]. For $Mn^{2+}$ ions with an electron spin $S = \frac{5}{2}$, there are five different $\Delta M = 1$ transitions, where $M$ is the electron spin quantum number. For an isotropic $g$ factor, transitions other than $\Delta M = +\frac{1}{2} \leftrightarrow -\frac{1}{2}$ strongly depend on the orientation with respect to the magnetic field and are typically not observed in powder samples. The $\Delta M = +\frac{1}{2} \leftrightarrow -\frac{1}{2}$ transition is split into a sextet by the hyperfine splitting of the Mn nuclear spin $I = \frac{5}{2}$. The $+\frac{1}{2}$, $m \leftrightarrow -\frac{1}{2}$, $m$

transitions with $\Delta m = 0$, where $m$ is the nuclear spin quantum number, are allowed transitions that give a sextet spectrum, and the $\Delta M = 1$, $\Delta m = 1$ transitions are forbidden transitions that show weak lines between the lines of the sextet. The sextet lines at high field are thus spaced apart because of the existence of significant zero-field interactions. An average hyperfine coupling constant $A$ of 95 G is obtained by averaging the five separations between successive hyperfine lines. Hence, the observed sextet EPR pattern with $g = 2.0147$ and $A = 95$ G corresponds to the $Mn^{2+}$ ion existing in a distorted octahedral coordination in the brucite-like layer. These EPR results are indeed similar to those observed in Mn–MCM-41 [24] and MnAPOs [25] with Mn extra-framework positions.

The EPR spectrum in Fig. 4(a) also shows two broad shoulders around 2800 G ($g \approx 2.5$) and 1700 G ($g \approx 4.1$). Similar low-field EPR peaks around $g = 3.2$ and 5.2 were observed in an Mn–MCM-41 material [24] and $g = 4.27$ in $Mn^{2+}$-exchanged ZSM-5. These EPR peaks were assigned to extra-framework $Mn^{2+}$ ions in a distorted tetrahedral symmetry. In view of these results it may be reasonable to assume that the $Mn^{2+}$ species in the brucite-like layer occupy a distorted octahedral and/or distorted tetrahedral coordination, or there should be more than one $Mn^{2+}$ species. As the Mn content in the sample increases, the EPR spectra show only a single line with $g \approx 2$ having a Lorentzian shape. The broadness of the line increases with a further increase in the Mn content. No hyperfine line is observed even for Mn 0.8-LDH, presumably because of the strong spin–spin interactions, namely the magnetic dipole interaction and the exchange interaction at this Mn concentration [26]. An exchange-narrowing interaction can thus account for the observed EPR spectrum of Mn 0.8-LDH and Mn 1.5-LDH [Fig. 4(b) and (c)]. It should be pointed out that all EPR lines observed in these samples correspond exclusively to the $Mn^{2+}$ species. No EPR signals can be assigned to the $Mn^{4+}$ species, as the observed $g$ values are around 2 and $>2$. These results are in contrast to those of Hansen and Taylor [13] on EPR of MgMn-LDHs without Al, which did not show any EPR signal, suggesting that all $Mn^{2+}$ ions in their samples were oxidized to $Mn^{3+}$.

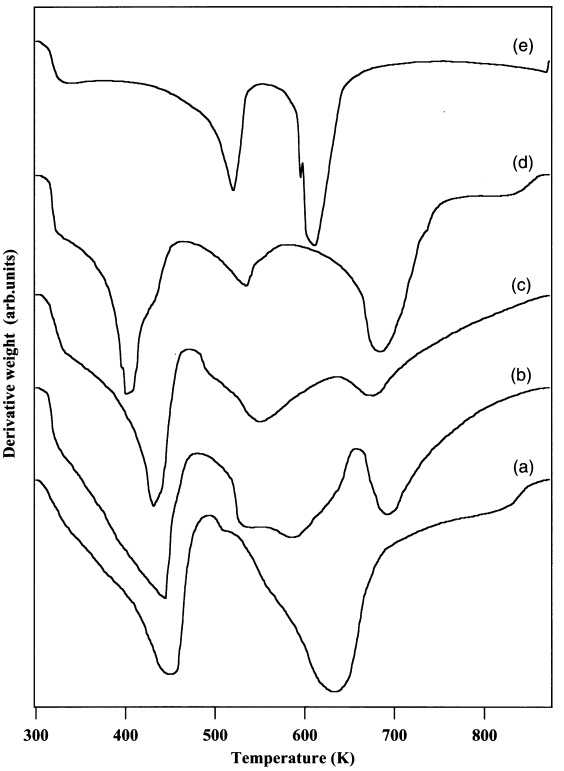


Fig. 5. DTG traces of (a) Mn 0.05-LDH, (b) Mn 1.0-LDH, (c) Mn 1.5-LDH, (d) Mn 2.0-LDH, (e) Mn 3.0-LDH.

The thermogravimetric (TG) analysis of MgAl-LDH without Mn exhibits two stages of weight loss [19]. The first weight loss $T_1$ occurs in the temperature range 423–523 K and has been attributed to the removal of interlayer water. The second weight loss $T_2$ recorded in the temperature range 623–723 K was ascribed to the removal of structural water and $CO_2$ by the decomposition of $CO_3^{2-}$ from the interlayer. The manganese-containing LDHs in the present study exhibited similar TG patterns with a net weight loss of about 40–50% up to 873 K. However, some differences in the number of stages of weight loss and their temperatures are noticed in the TG patterns upon incorporation of manganese. For the sake of clarity, the derivatives of the TG (DTG) curves are presented in Fig. 5. It can be noticed from these

figures that the temperature of the $T_1$ process decreases from 440 K for Mn 0.05-LDH to 395 K for Mn 2.0-LDH. On the other hand, an upward shift in the $T_2$ process from sample Mn 0.05-LDH (630 K) to Mn 2-LDH (690 K) is observed. Furthermore, an additional weight loss process between $T_1$ and $T_2$ is noticed. Mn 3.0-LDH, without Mg [which consists of a mixture of $Mn(OH)_2$ and $MnCO_3$], exhibits two peaks, one at 524 K and the other at 619 K, that are attributed to the decomposition of $Mn(OH)_2$ [29] and $MnCO_3$ [30].The lowering of $T_1$ with increasing Mn content could be ascribed to a decrease in crystallinity of the compound (cf. XRD), which would facilitate the removal of interlayer water at relatively low temperatures. The increase in the decomposition temperature $T_2$ with increasing Mn content can be attributed to an increase in the electrostatic attractive forces between the brucite-like layer and the interlayer as a result of isomorphous substitution of Mn ions, probably as $Mn^{3+}$ in addition to $Mn^{2+}$, in the MgAl-LDH framework. This argument is supported by the UV–Vis DRS and the XRD results, wherein the calculated $c$ parameter decreases with increasing Mn content (Table 1). The additional weight loss process observed between $T_1$ and $T_2$ in the range 520–660 K could be due to the decomposition of impurity phases such as $Mn(OH)_2$ and $MnCO_3$, since this temperature range matches well with that of the decomposition of the $Mn(OH)_2$ and $MnCO_3$ phases in Mn 3.0-LDH. However, Zeng et al. [31] noticed additional weight loss processes around 540 K and 580 K in MgCo-LDHs, and they assigned these peaks to the decomposition of $NO_3^-$ and $CO_3^{2-}$ respectively.

Based on the results obtained from XRD, FT-IR, UV–Vis DRS, EPR and thermal analysis (TG/DTG), it can be concluded that only a part of the $Mn^{2+}$ is oxidized to $Mn^{3+}$ during the synthesis and post-synthesis treatments (ageing and drying). Probably, the majority of the Mn species retain their $+2$ oxidation state. This is in contrast to earlier results obtained with $Mg^{2+}Mn^{3+}$-LDHs prepared by air oxidation and co-precipitation methods, where most of the $Mn^{2+}$ ions were oxidized to $Mn^{3+}$. The structure of the MgMnAl-LDHs in the present system can thus be represented schematically as in Fig. 6. Both $Mn^{2+}$ and $Mn^{3+}$ are shown to be incorporated in the MgAl-LDH framework. The following general formula can be proposed for these LDH materials with incorporated manganese:

$Mg_{6-(x+y)}(Mn^{2+})_x(Mn^{3+})_yAl_2(OH)_{16}[(y+2)/2]CO_3 \cdot nH_2O$, where $(x+y) \leq 0.8$. Unfortunately, from our experimental results, it was not possible to estimate quantitatively the $Mn^{2+}/Mn^{3+}$ ratio that has been incorporated in the layers of MgAl-LDHs.

The $N_2$ adsorption–desorption isotherms of

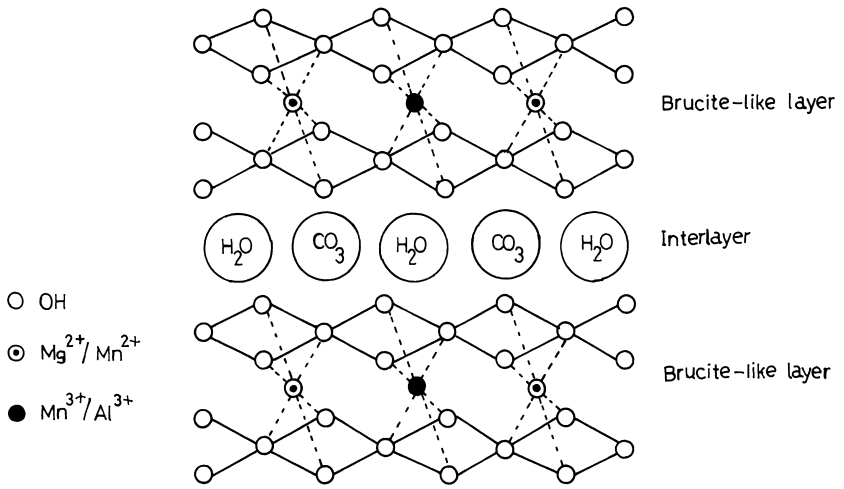


Fig. 6. Schematic structural representation of MgMnAl-LDH.

these samples corresponded to the type IV in the IUPAC classification [32]. The specific surface areas of these samples (Table 1) are in the range 40 to 60 $m^2 g^{-1}$, and the specific pore volumes varied from 0.2 to 0.3 $cm^3 g^{-1}$.

### 3.2. Characterization of the calcined Mn-LDHs

Calcination of the LDHs results in the destruction of the layer structure, and various metastable phases are formed depending upon the calcination temperature [33]. The identification of crystalline phases formed during calcination at various temperatures is useful to assess the thermal stability of the compounds. For this purpose, the sample Mn 0.05-LDH was subjected to calcination at various temperatures for 5 h in air. We employed both XRD and EPR techniques to understand the nature of the phases formed and the chemical environment of Mn species present in the calcined samples. Fig. 7 shows the XRD patterns of Mn 0.05-LDH calcined at various temperatures. The removal of physisorbed water at 423 K does not modify the layer structure. Only a small decrease in the basal spacing [$d(003)$; $2\theta \approx 12^\circ$] from 7.65 Å to 7.46 Å is noticed, indicating that a minor amount of interlayer water is lost at this temperature. At a calcination temperature of 573 K the dehydration process (as evidenced from TG/DTG) induces a decrease in basal spacing of about 1 Å (a shift from 7.46 to 6.40 Å). At the same time the $(10l)$ reflections at higher $2\theta$ angle are also shifted and become broader due to some disorder in the structure that still retains the characteristics of a layer structure. The original LDH structure is retained up to around 573 K. However, for the sample calcined at 723 K, the absence of diffraction peaks corresponding to an LDH phase reveals that the layer structure is completely destroyed due to the removal of structural water and $CO_2$ from the interlayer (the $T_2$ process in TG). This also caused an increase in surface area from 60 $m^2 g^{-1}$ to around 200 $m^2 g^{-1}$ and the specific pore volume from about 0.3 $cm^3 g^{-1}$ to 0.7 $cm^3 g^{-1}$. For this calcination temperature two broad diffraction lines are observed that correspond to the $d(200)$ and $d(220)$ reflections of a mixed oxide phase with MgO-like structure. The lattice constant of the MgO-like phase has been calculated to be 4.220 Å, which is higher than that of pure MgO (4.211 Å; JCPDS file no. 45-946). The increase in the lattice parameter in the present system reveals that some $Mn^{2+}$ ions are dissolved in the MgO lattice to form a solid solution (vide infra). The sharpness of the XRD peaks increases further upon increasing the calcination temperature to 1073 K, in line with a progressive increase in the crystallinity of the MgO-like phase. In addition, diffraction peaks corresponding to $MgAl_2O_4$ spinel [Fig. 7(e)] are observed at this temperature. Very sharp and well-defined crystalline phases of MgO and $MgAl_2O_4$ are obtained at 1473 K.

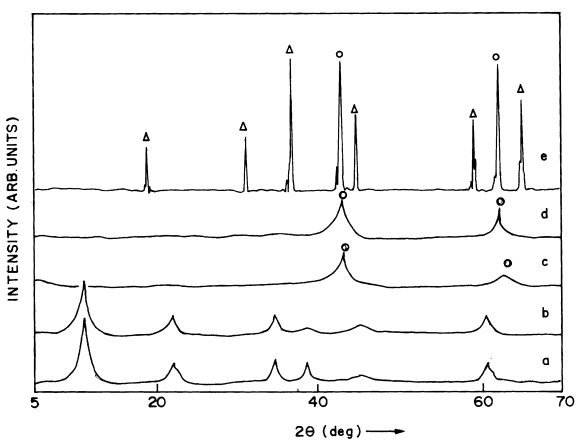


Fig. 7. XRD patterns of Mn 0.05-LDH calcined at various temperatures: (a) 423 K; (b) 573 K; (c) 723 K; (d) 1073 K; (e) 1473 K. Peaks corresponding to MgO and $MgAl_2O_4$ phases are marked by ○ and △ respectively.

Fig. 8 presents the EPR spectra of Mn 0.05-LDH calcined at various temperatures. All samples show six hyperfine lines similar to those observed in the as-synthesized sample. The $g$ factors of these sextet EPR patterns are centered around 2.0 with an average hyperfine coupling constant $A$ of 80–90 G (see Table 3) indicating that the Mn in these samples retains its +2 oxidation state, even upon calcination. However, differences are observed in the EPR line intensities as well as in the spectral parameters. Removal of interlayer water at 573 K results in a decrease in the EPR line intensities [cf. Figs. 4(a) and 8(a)]. A significant loss in intensity and resolution of the EPR lines is observed when the sample is calcined

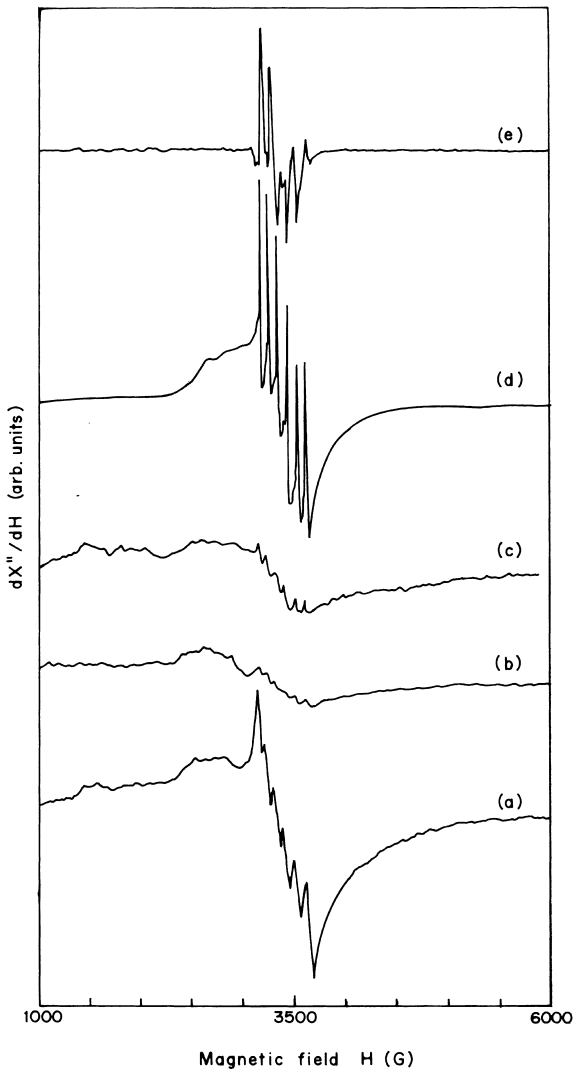


Fig. 8. EPR spectra of Mn 0.05-LDH calcined at various temperatures: (a) 573 K; (b) 723 K; (c) 1073 K; (d) 1473 K; (e) 1473 K measured at 77 K.

at 723 K. Furthermore, the low-field shoulders (assigned to tetrahedral $Mn^{2+}$) that are observed around 2600 G ($g \approx 2.5$) and 1600 G ($g \approx 4.4$) in the as-synthesized sample become more pronounced in the samples calcined up to 723 K. It should be noted that the dehydration and decarbonation of LDHs is taking place in this temperature range (from XRD and TG results). Such a dehydration and decarbonation process would facilitate the transformation of the coordination

Table 3
EPR parameters of the $Mn^{2+}$ ion in Mn 0.05-LDH calcined at various temperatures

| Calcination temperature (K) | $g$ factor | $A$ (G) |
|---|---|---|
| 573 | 2.0642 | 92.8 |
| 723 | 2.0704 | 88.3 |
| 1073 | 2.0680 | 87.3 |
| 1473 | 2.0449 | 88.6 |
| 1473[a] | 2.0634 | – |

[a] Measured at 77 K.

of $Mn^{2+}$ ion (probably from octahedral to tetrahedral) similar to the phenomenon well known for $Al^{3+}$ in the brucite-like layer [7,19]. The XRD of the sample calcined at 723 K indicates that $Mn^{2+}$ ions are present in the poorly crystalline MgO-like solid solution. Hence the observed EPR lines in Fig. 8(b) correspond to $Mn^{2+}$ ions dissolved in the MgO-like solid solution. A further increase in the calcination temperature to 1073 K results in an increase in the EPR line intensity, perhaps because of the increase in crystallinity of the solid solution as evidenced by XRD. A sharp, well-resolved and highly intense six-line EPR pattern is recorded at 1473 K. Also, one of the low-field EPR lines around 1600 G has vanished. In addition, the spectrum clearly shows several small shoulders due to the forbidden transitions, as explained for the as-synthesized sample. It should be recalled that the XRD pattern of the sample showed a mixture of a well-crystallized MgO solid solution and $MgAl_2O_4$ spinel phases. The $Mn^{2+}$ ions in the MgO solid solution are thus immobilized [23–25]. When the EPR of the same sample was measured at low temperature (77 K), the weak forbidden transitions, apparent in the room temperature measurement, became averaged [Fig. 8(e)]. The spectral spacing and the line intensities became unequal because of the large zero-field interactions. Furthermore, the broad shoulder around $g \approx 2.6$ is now completely absent. These results reveal that, at low temperature (77 K), all $Mn^{2+}$ ions have a similar chemical environment, mostly in a distorted octahedral coordination, and the $Mn^{2+}$ ions are further immobilized in the MgO-like lattice.

LDHs have been employed as catalysts either

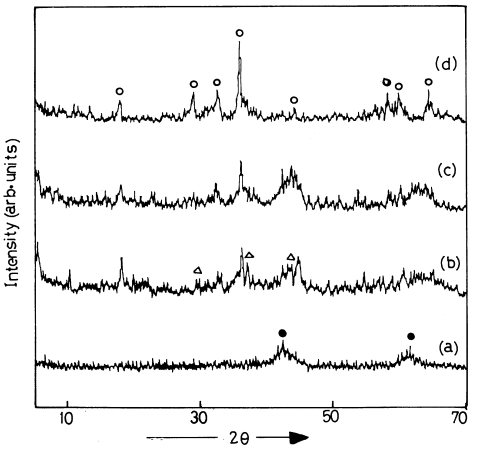


Fig. 9. XRD patterns of MgMnAl-LDH calcined at 723 K for 4 h in air: (a) Mn 0.05-LDHcal; (b) Mn 0.8-LDHcal; (c) Mn 1.5-LDHcal; (d) Mn 3.0-LDHcal. Peaks corresponding to the MgO, $Mn_3O_4$ and $MnAl_2O_4$ phases are marked by ●, ○ and △ respectively.

as such or after a controlled thermal treatment, generally around 723 K [34–36]; for recent catalytic applications of HT-like clays see Ref. [37]. At this temperature LDHs lose their layer structure and form highly active mixed oxides with high thermal stability, high surface area and good metal dispersion, properties that are very important for their catalytic applications [34]. Hence it is important to study the nature of the products formed during calcination of Mn-containing LDHs at 723 K (hereinafter referred to as Mn $x$-LDHcal). The XRD patterns of some of the Mn-incorporated LDHs calcined at 723 K for 4 h are shown in Fig. 9. It can be seen that these calcined products are poorly crystalline metal oxides. The sample with the lowest Mn content (Mn 0.05-LDHcal) is a cubic phase corresponding to MgO. No other Al- or Mn-containing phases are detected, but they are probably present in small quantities or in X-ray amorphous forms.

It has been reported by several authors [19,33,34] that, in the case of MgAl-LDHs, thermal decomposition around 723 K yields a poorly crystalline MgO phase whose lattice constant $a$ is less than that of pure MgO. The result has been attributed to the dissolution of a small amount of $Al^{3+}$ in the MgO lattice to form solid solutions. The chemical composition of the resulting solid solution is given by the formula $Mg_{(1-x)/(2+x)}Al_{2x/(2+x)}[\,]_{x/(2+x)}O$, where [ ] is a cation vacancy created due to the dissolution of part of the $Al^{3+}$ in the MgO lattice [38]. In contrast, the lattice parameter $a$ of the resulting MgO phase of Mn 0.05-LDHcal was calculated to be 4.220 Å from the $d(200)$ and $d(220)$ planes. The increase in the $a$ value of the resulting MgO-like phase in the present system indicates that some amount of $Mn^{2+}$ is dissolved in the MgO lattice to form Mg–O–Mn or Mg–O–Al/Mn solid solutions similar to the composition described above. As the Mn content increases, in addition to MgO, other Mn-containing phases crystallize. Nevertheless, the broadness of the XRD peaks makes it difficult to assign them to well-defined phases. However, the spinel phase corresponding to $Mn_3O_4$ (hausmannite; JCPDS file no. 24-734) can be easily identified, as its crystallinity increases further with increasing Mn content, and it is the major phase recorded in Mn 3.0-LDHcal. Among other possible phases, the diffraction peaks fit better for $MnAl_2O_4$ spinel (galaxite; JCPDS file no. 29-880). Taking into account the oxidation states of cations existing in these spinel materials $Mn_3O_4$ $[Mn^{2+}(Mn^{3+})_2O_4]$ and $MnAl_2O_4$ $[Mn^{2+}(Al^{3+})_2O_4]$, the approximate ratio of $Mn^{2+}/Mn^{3+}$ would be 2:2. This means that approximately 50% of the manganese is present as $Mn^{3+}$ ions in the samples calcined at 723 K, whereas the rest of the Mn retains its +2 oxidation state. This is in contrast to the results reported by Fernandez et al. [14] who calcined MgMn-LDH, wherein a mixture of MgO and $Mg_2MnO_4$ spinel (manganese is in the +4 oxidation state) phases are observed at calcination temperatures in the range from 663 to 1273 K.

It is known in the literature [39] that a higher Mg/Mn atomic ratio of about 6 is necessary for the formation of a pure $Mg_2MnO_4$ spinel phase. However, Fernandez et al. [14] observed it during calcination of the MgMn-LDH (Mg/Mn = 3.03). In contrast, this phase was not detected even in Mn 0.8-LDH, in which the Mg/Mn ratio (2.75) was close to that of 3.03 in MgMn-LDH. This is perhaps due to the co-presence of Al in our precursor material (LDH), which could partially prevent the oxidation of $Mn^{2+}$. This is possible if

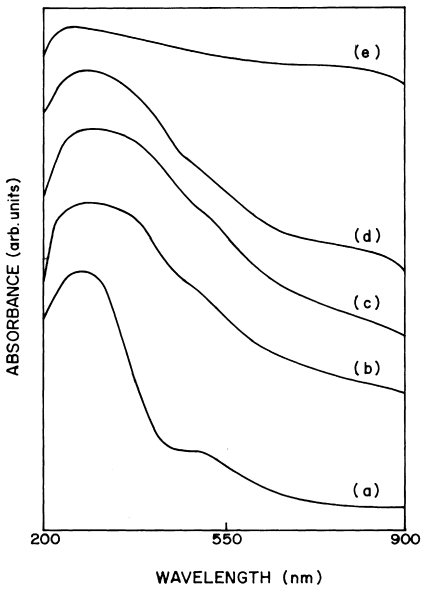


Fig. 10. UV–Vis DRS of MgMnAl-LDHs calcined at 723 K for 4 h in air: (a) Mn 0.05-LDHcal; (b) Mn 1.0-LDHcal; (c) Mn 1.5-LDHcal; (d) Mn 2.0-LDHcal; (e) Mn 3.0-LDHcal.

the $Mn^{2+}$ phase is decorated by an Al-containing phase, as described previously for the sintering of $NiAl_2O_4$ spinel [7]. The formation of the $MnAl_2O_4$ phase in the present study is not surprising, as in many cases the $M^{2+}$–$M^{3+}$ spinel is obtained upon calcination above 723 K (e.g. $MgAl_2O_4$ from MgAl-LDH, $NiAl_2O_4$ from NiAl-LDH, $ZnAl_2O_4$ from ZnAl-LDH [34]). Moreover, the $MnAl_2O_4$ spinel can be obtained by heating a mixture of $Mn_3O_4$ and $\alpha$-$Al_2O_3$ in air at 1823 K for 24 h (JCPDS file no. 29-880).

The UV–Vis DRS results of some of the Mn-containing samples calcined at 723 K are shown in Fig. 10. Although the spectral patterns look similar to those of the as-synthesized samples, several major differences are clearly seen:

1. all absorption bands (except in Mn 3.0-LDH) are very intense, and the band around 250 nm is even more intense and broad compared with those of the as-synthesized samples;
2. the compound with very low Mn content (Mn 0.05-LDH) exhibits a broad band in the range 250–320 nm together with a weak band around 500 nm.

The appearance of a broad band between 250 and 320 nm in Mn 0.05-LDHcal could be due to the $O^{2-} \rightarrow Mn^{2+}$ charge transfer transition superimposed on the $O^{2-} \rightarrow Mn^{3+}$ charge transfer transition (see Table 2). The weak bands observed around 480 and 500 nm are due to the $Mn^{3+}$ and $Mn^{2+}$ d–d transitions superimposed on the above charge transfer bands. These results reveal that partial oxidation of $Mn^{2+}$ to $Mn^{3+}$ takes place upon calcination of the samples, even of those with a very low Mn content. However, XRD indicates that the compound is a poorly crystalline MgO-like solid solution; the presence of an $Mn^{3+}$-containing phase, such as $Mn_3O_4$, is not detected even though it may be existing as an amorphous phase. The appearance of a sextet in the EPR spectrum and an increased lattice constant support the contention that the $Mn^{2+}$ ion rather than the $Mn^{3+}$ is dissolved in the MgO-like lattice to form a solid solution. The compound Mn 3.0-LDHcal, which consists of $Mn_3O_4$ spinel as the major phase, exhibits very strong absorption bands in the whole region of the spectrum, presumably because of the random distribution of $Mn^{2+}$ and $Mn^{3+}$ ions in the mixed oxide phase. Hence, from the results of XRD, EPR and UV–Vis DRS it can be concluded that calcination of Mn 0.05-LDH at various temperatures generates phases similar to those of a simple MgAl-LDH system. Partial oxidation of $Mn^{2+}$ to $Mn^{3+}$ takes place during calcination. Manganese exists as $Mn^{2+}$ ion in the MgO-like solid solution and retains its $+2$ oxidation state even at very high calcination temperatures (1473 K). As the Mn content increases, in addition to the MgO-like phase, spinel phases such as $Mn_3O_4$ and $MnAl_2O_4$ are formed, and an $Mn^{2+}/Mn^{3+} \sim 1$ is obtained in the calcined LDHs (at 723 K).

### 3.3. Catalytic oxidation of toluene

#### 3.3.1. Influence of the Mn content

In order to demonstrate the potential usefulness of these Mn-containing LDHs, the liquid-phase oxidation of toluene was carried out as a test reaction using TBHP as an oxidant. The oxidation of toluene to benzoic acid is an important industrial process [40], and toluene is the cheapest aromatic hydrocarbon [41].

Table 4
Toluene oxidation over various MgMnAl-LDHs[a]

| Catalyst | Toluene conversion (mass%) | Rate of toluene conversion (mmol $h^{-1}$ $g^{-1}$) | Product selectivity (mass%) | | |
|---|---|---|---|---|---|
| | | | Benzaldehyde | Benzyl alcohol | Benzoic acid |
| Mn 0.05-LDH | 1.5 | 0.4 | 100 | – | – |
| Mn 0.8-LDH | 6.0 | 1.6 | 62.7 | 1.8 | 35.5 |
| Mn 1.0-LDH | 8.3 | 2.2 | 43.8 | 6.0 | 50.3 |
| Mn 1.5-LDH | 11.3 | 3.0 | 32.1 | 11.9 | 56.0 |
| Mn 2.0-LDH | 14.3 | 3.8 | 23.9 | 1.1 | 75.0 |
| Mn 3.0-LDH | 3.4 | 0.9 | 23.6 | 1.9 | 74.5 |

[a] Reaction conditions: solvent, acetonitrile; toluene:TBHP = 1:4; reaction temperature, 353 K; reaction time, 4 h.

The liquid-phase oxidation of toluene can lead to various products. Oxidation of the side chain and/or the aromatic ring takes place depending upon the nature of the catalyst employed. Ti-silicalites (TS-1) have been found to favor the hydroxylation of toluene to give a mixture of cresols [42]. On the other hand, V-silicalites (VS-1) [43] or Cr-silicalites (CrS-1) [44] favor the side chain oxidation of toluene to a mixture of benzaldehyde, benzyl alcohol, benzoic acid and dibenzyl. In the present study, the oxidation of toluene over Mn-containing LDHs gave only benzaldehyde and benzoic acid as the major products, with minor amounts of benzyl alcohol. Preliminary runs were performed in order to choose a suitable toluene:TBHP ratio, and it was found that the optimum ratio was 1:4. MgAl-LDH, without Mn, was found to be inactive in the oxidation of toluene. Table 4 summarizes the results of the catalytic oxidation of toluene over a series of MgMnAl-LDHs. It can be observed that the rate of toluene conversion and the selectivity to benzoic acid increase with increasing Mn content in the sample. This indicates that the rate of oxidation of toluene to benzaldehyde and the subsequent oxidation to benzoic acid increase as the Mn content in the sample increases. It is also noticed that when Mg in the LDH is completely replaced by Mn (Mn 3.0-LDH), its catalytic activity for the toluene conversion is less compared with the other Mn-substituted analogues. As the XRD of the sample showed the existence of phases corresponding to $Mn(OH)_2$ and $MnCO_3$ rather than the LDH phase, it appears that the Mn existing in the LDH phase is catalytically more active for toluene oxidation. It is worth mentioning here that the MnAPOs were found to be inactive for similar oxidation reactions [45].

### 3.3.2. Effect of solvents

The influence of the polarity of the solvent on the catalytic activity was also investigated. Since the catalyst Mn 2.0-LDH showed the highest rate of toluene conversion and the highest selectivity for benzoic acid, this catalyst was employed to investigate the effect of the solvent on the catalytic performance. Three solvents, viz. $CCl_4$, a non-polar (dielectric constant $\epsilon = 2.23$) aprotic solvent, acetonitrile, a more polar ($\epsilon = 36.2$) aprotic solvent and *tert*-butanol, a moderately polar ($\epsilon = 10.9$) protic solvent were employed [46]. The results (Table 5) indicate that the nature of the solvent has a strong influence on the toluene conversion, as well as on the product selectivity. The conversion of toluene increases with increasing dielectric constant of the solvent, whereas the influence of the polarity on the product distribution is complex. Comparing the product selectivities obtained in $CCl_4$ and acetonitrile (aprotic solvents), it is observed that the increase in the dielectric constant of the solvent from 2.23 (for $CCl_4$) to 36.2 (for acetonitrile) enhances the selectivity for benzoic acid from about 40% to around 75%. This is because of the fact that a polar solvent is preferred to form a polar product [47]. On the other hand, the protic solvent *tert*-butanol seems to favor the formation of benzaldehyde, whereas the non-polar, aprotic solvent favors the formation of benzyl

Table 5
Effect of solvent on toluene oxidation over Mn 2.0-LDH[a]

| Solvent used | Toluene conversion (mass%) | Rate of toluene conversion (mmol $h^{-1}$ $g^{-1}$) | Product selectivity (mass%) | | |
|---|---|---|---|---|---|
| | | | Benzaldehyde | Benzyl alcohol | Benzoic acid |
| $CCl_4$ | 3.8 | 1.0 | 37.8 | 18.2 | 43.9 |
| *tert*-Butanol | 9.0 | 2.4 | 60.0 | – | 42.0 |
| Acetonitrile | 14.3 | 3.8 | 23.9 | 1.1 | 75.0 |

[a] Reaction conditions: toluene:TBHP = 1:4; reaction temperature, 353 K; reaction time, 4 h.

alcohol. Further investigations are in progress in order to understand the reasons for the above selectivity differences.

## 4. Conclusions

Our study indicates that nearly 20% of the metal ions in the MgAl-LDH can be isomorphously substituted by $Mn^{2+}/Mn^{3+}$ ions to obtain a single phase corresponding to an Mg–Mn–Al ternary-LDH (Mn 0.8-LDH). Only a part of $Mn^{2+}$ is oxidized to $Mn^{3+}$ during the synthesis and post-synthesis treatments such as ageing and drying. Probably, the majority of the $Mn^{2+}$ ions exist in a distorted octahedral coordination or in more than one chemical environment in the MgAl-LDH framework, thereby generating a new material with the general formula $Mg_{6-(x+y)}(Mn^{2+})_x(Mn^{3+})_yAl_2(OH)_{16}[(y+2)/2]CO_3 \cdot nH_2O$, where $(x+y) \leq 0.8$.

Calcination of the Mn-containing LDHs at 723 K results in the formation of spinel phases, such as $Mn_3O_4$ and $MnAl_2O_4$, along with an MgO-like phase. Partial oxidation of $Mn^{2+}$ to $Mn^{3+}$ takes place during calcination. Hence, nearly 50% of the $Mn^{2+}$ is oxidized to $Mn^{3+}$ upon calcination in air at 723 K, whereas the rest of the manganese is retained in the $+2$ oxidation state. The material with a very low Mn content retains Mn in its $+2$ oxidation state (EPR-active) even upon calcination in air at very high temperature (1473 K), and the $Mn^{2+}$ ions are immobilized in the MgO-like lattice in a distorted octahedral environment.

The as-synthesized samples can be used as catalysts for the liquid-phase oxidation of toluene to produce selectively benzaldehyde/benzoic acid. The catalytic activity increases with increasing Mn content in the LDH. The $Mn^{2+}/Mn^{3+}$ ions present in the LDH structure show better catalytic performance than a mixture of $Mn(OH)_2$ and $MnCO_3$. The nature of the solvent plays a crucial role in the catalytic performance. An increase in the solvent polarity brings about an enhanced rate of toluene conversion and a better selectivity for benzoic acid.

## References

[1] H. Cao, S.L. Suib, J. Am. Chem. Soc. 116 (1994) 5334.
[2] E. Libby, J.K. McCusker, E.A. Schmitt, K. Folting, D.N. Hendrickson, G. Christou, Inorg. Chem. 30 (1991) 3486.
[3] I.S. Singoredjo, R.B. Korrer, F. Kapteijn, S.A. Moulijn, Appl. Catal. B: Environ. 1 (1992) 297.
[4] S.L. Brock, N. Duan, Z.R. Tian, O. Giraldo, H. Zhou, S.L. Suib, Chem. Mater. 10 (1998) 2619.
[5] M. Bellotto, G. Artioli, C. Cristiani, P. Forzatti, G. Groppi, J. Catal. 179 (1998) 597.
[6] A. Vaccari, Catal. Today 41 (1998) 53.
[7] M. Bellotto, B. Rebours, O. Clause, J. Lynch, D. Bazin, E. Elkaim, J. Phys. Chem. 100 (1996) 8527.
[8] F. Basile, L. Basini, G. Fornasari, M. Gazzano, F. Trifiro, A. Vaccari, J. Chem. Soc. Chem. Commun. (1996) 2435.
[9] A. de Roy, A.C. Forano, F. Eimalki, J.P. Besse, in: M.L. Ocelli, H.F. Robson (Eds.), Expanded Clays and other Microporous Solids, Van Nostrand–Reinhold, New York, 1992, p. 108.
[10] S. Velu, A. Ramani, B.M. Chanda, S. Sivasanker, J. Chem. Soc. Chem. Commun (1997) 2107.
[11] S. Velu, K. Suzuki, T. Osaki, F. Ohashi, S. Tomura, Mater. Res. Bull. (1999) in press.
[12] P.J. Dunn, D.R. Peacot, T.D. Palmer, Am. Mineral. 64 (1979) 127.
[13] H.C.B. Hansen, R.M. Taylor, Clay Miner. 26 (1991) 507.
[14] J.M. Fernandez, C. Barriga, M.A. Ulibarri, F.M. Labajos, V. Rives, J. Mater. Chem. 4 (1994) 1117.
[15] S. Velu, C.S. Swamy, J. Mater. Sci. Lett. 15 (1996) 1674.

[16] K. Kuma, W. Paplowsky, B. Gedulin, G. Arrhenius, Orig. Life Evol. Biosph. 19 (1989) 537.
[17] B.E. Douglas, D.H. McDaniel, J.J. Alexander, Concepts and Models of Inorganic Chemistry, 2nd edition, Wiley, New York, 1983.
[18] R.D. Shannon, Acta Crystallogr. Sect. A: 32 (1976) 751.
[19] S. Velu, D.P. Sabde, N. Shah, S. Sivasanker, Chem. Mater. 10 (1998) 3451.
[20] G.W. Pratt, R. Coelho, Phys. Rev. 116 (1959) 281.
[21] F. Milella, J.M. Gallardo-Amores, M. Baldi, G. Busca, J. Mater. Chem. 8 (1998) 2525.
[22] W.S. Kijlstra, E.K. Poels, A. Bliek, B.M. Weckhuysen, R.A. Schoonheydt, J. Phys. Chem. B 101 (1997) 309.
[23] D. Zhao, D. Goldfarb, J. Chem. Soc. Chem. Commun. (1995) 875.
[24] X.Z. Luan, T. Wasowicz, L. Kevan, Micropor. Mesopor. Mater. 22 (1998) 179.
[25] Z. Levi, A.M. Raitsimring, D. Goldfarb, J. Phys. Chem. 95 (1991) 7830.
[26] G. Brouet, X. Chen, C.W. Lee, L. Kevan, J. Am. Chem. Soc. 114 (1992) 3721.
[27] J.C. Vedrine, in: F. Delannay (Ed.), Characterization of Heterogeneous Catalysts, Marcel Dekker, New York, 1984, p. 161.
[28] B. Wichterlova, S. Beran, S. Bednarova, K. Nedomova, K. Dudikova, P. Jiru, Innovation in zeolite materials science, in: P.J. Grobet, W.J. Mortier, E.F. Vansant, G. Schulz-Ekloff (Eds.), Studies in Surface Science and Catalysis, vol. 37, Elsevier, Amsterdam, 1988, p. 199.
[29] R.C. Weast (Ed.), Handbook of Chemistry and Physics, CRC Press, FL, USA, 1980, p. B-217.
[30] R.C. Weast (Ed.), Handbook of Chemistry and Physics, CRC Press, FL, USA, 1980, p. B-216.
[31] H.C. Zeng, Z.P. Xu, M. Qian, Chem. Mater. 10 (1998) 2277.
[32] G. Leofanti, M. Padovan, G. Tozzola, B. Venturelli, Catal. Today 41 (1998) 207.
[33] J.M. Fernandez, C. Barriga, M.A. Ulibarri, F.M. Labajos, V. Rives, Chem. Mater. 9 (1997) 312.
[34] F. Cavani, F. Trifiro, A. Vaccari, Catal. Today 11 (1991) 173.
[35] S.M. Auer, R. Wandeler, U. Gobel, A. Baiker, J. Catal. 169 (1997) 1.
[36] F. Basile, L. Basini, M.D. Amore, G. Fornasari, A. Guarinoni, D. Matteuzzi, G.D. Piero, F. Trifiro, A. Vaccari, J. Catal. 173 (1998) 247.
[37] Appl. Clay Sci. 13 (1998) 311–511.
[38] V.R.L. Constantino, T.J. Pinnavaia, Catal. Lett. 23 (1994) 361.
[39] H. Tarssaint, Rev. Chim. Mineral. 1 (1964) 141.
[40] W. Jordan, H. van Barneveld, O. Gerlich, M. Kleine-Boymann, J. Ullrich, in: B. Elvers, S. Hawkins, G. Schulz (Eds.), Phenol, Ullmann's Encyclopedia of Industrial Chemistry vol. A19, VCH, Weinheim, 1991, p. 304.
[41] J. Fabri, U. Graeser, T.A. Simo, in: B. Elvers, S. Hawkins (Eds.), Toluene, Ullmann's Encyclopedia of Industrial Chemistry vol. A27, VCH, Weinheim, 1996, p. 147.
[42] G.N. Vayssilov, Z. Popova, S. Bratinova, A. Tuel, in: R.K. Grasselli, S. Toyoma, A.M. Gaffney, J.E. Lyons (Eds.), Third World Congress on Oxidation Catalysis, Studies in Surface Science and Catalysis vol. 110, Elsevier, Amsterdam, 1997, p. 9.
[43] C. Marchal, A. Tuel, Y. Ben Taarit, in: M. Guisnet, J. Barbier, J. Barrault, C. Bouchoule, D. Duprez, G. Perot, C. Montassier (Eds.), Heterogeneous Catalysis and Fine Chemicals III, Studies in Surface Science and Catalysis vol. 78, Elsevier, Amsterdam, 1993, p. 447.
[44] A.P. Singh, T. Selvam, J. Mol. Catal. A: Chem. 110 (1996) 489.
[45] R.A. Sheldon, in: R.K. Grasselli, S. Toyoma, A.M. Gaffney, J.E. Lyons (Eds.), Third World Congress on Oxidation Catalysis, Studies in Surface Science and Catalysis vol. 110, Elsevier, Amsterdam, 1997, p. 151.
[46] A.J. Gordon, R.A. Ford, in: The Chemist's Companion, A Handbook of Practical Data, Techniques and References, Wiley, New York, 1972, pp. 1–30.
[47] R. Yu, F. Xia, D. Wang, Y. Liu, G. Pang, S. Feng, S. Qui, R. Xu, Catal. Lett. 49 (1997) 49.